Computational Mechanics
https://doi.org/10.1007/s00466-024-02570-5

ORIGINAL PAPER

Third-order geometric stiffness formulation for improved mesh convergence of thin and wide spatial beams in the generalized strain beam formulation

M. Nijenhuis[1] · J. P. Meijaard[1] · M. Naves[1,3] · R. G. K. M. Aarts[2]

Received: 1 May 2024 / Accepted: 9 October 2024

Abstract
This paper presents the stiffness formulation of a beam element with the relevant third-order nonlinear geometric effects for relatively wide and thin rectangular beams, in particular when loaded in the plane and simultaneously deformed out of the plane. The element is initially straight in its undeformed configuration. The formulation is based on Timoshenko beam theory with nonuniform torsion and Wagner effects. The derivation is carried out by means of the Hellinger–Reissner variational principle with custom interpolation functions. The element is incorporated into the generalized strain beam formulation for multibody systems. Numerical simulations of precision flexure mechanisms show that the use of a single third-order element per flexible member can already yield adequate performance, at a significant reduction of the necessary degrees of freedom and the computation time, compared with using multiple second-order elements in the generalized strain beam formulation.

Keywords Geometric stiffness · Sheet flexure · Mesh convergence · Beam element · Variational principle · Wide thin beam

1 Introduction

In the stiffness analysis of deforming structures, the third-order terms in the load–displacement relationship can have a significant effect, especially in high aspect ratio structures such as thin and wide beams. Examples are the so-called sheet flexures or leaf springs in flexure mechanisms used for precision manipulation [14, 20, 49, 50]. Because the thickness is generally two orders of magnitude smaller than the width and length, a sheet flexure has a plate-like geometry, meaning that it can be used to provide a high stiffness against loads acting in its geometric middle plane while simultaneously undergoing moderate elastic deformation in the out of plane direction. From a design point of view, an accurate description of the in-plane stiffness in the deformed configuration is a relevant performance metric of flexure mechanisms. It can be obtained with numerical implementations of various plate or beam theories. To facilitate the design optimization of flexure mechanisms that consist of a multitude of sheet flexures, we aim to reduce the computational effort by refining the stiffness description of an existing beam element, so that fewer elements are required for mesh convergence.

This work concerns the stiffness refinement of an existing second-order beam element in the generalized strain beam formulation, such that a single such complex element can yield a similarly accurate description as multiple simpler elements, and with lower total computational effort. Since lowering the computational effort is a motivation for this work, we choose to develop a beam element instead of a plate element because of its smaller number of coordinates.

In this paper, we present the stiffness formulation for a numerical element with the third-order effects that are relevant for wide and thin rectangular beams. The element is assumed to be straight in the undeformed configuration.

✉ M. Nijenhuis
m.nijenhuis@utwente.nl

J. P. Meijaard
j.p.meijaard@utwente.nl

M. Naves
m.naves@windesheim.nl

R. G. K. M. Aarts
r.g.k.m.aarts@utwente.nl

[1] Precision Engineering, Faculty of Engineering Technology, University of Twente, Enschede, The Netherlands

[2] Applied Mechanics & Data Analysis, Faculty of Engineering Technology, University of Twente, Enschede, The Netherlands

[3] Industrial Automation & Robotics, University of Applied Sciences Windesheim, Zwolle, The Netherlands

Published online: 11 November 2024

The stiffness formulation is based on the analytical closed-form model that was presented in Ref. [37]. The element is incorporated into the generalized strain beam formulation for multibody systems [7, 21]. A key aspect of the formulation is the use of generalized strain and stress parameters, alongside the common nodal coordinates and loads. The generalized strain beam formulation is suited for the simulation of multibody systems that consist of both rigid and flexible elements, since the retention of the discretized strains (the generalized strains) in the equations to be solved enables a natural specification of element rigidity (by setting the generalized strains to a zero value) and element flexibility (by providing constitutive relations between the generalized strains and stresses). Various types of elements have been formulated, such as truss, hinge, tube, wheel and beam elements [30, 43]. The beam element with a second-order stiffness description [22, 24, 29], based on Timoshenko beam theory, serves as a basis for the current work.

The derivation of the third-order terms that appear in the load–displacement relations is carried out in a corotational frame by means of the Hellinger–Reissner variational principle [56] with a specific set of displacement and stress interpolation functions: an explicit dependency of the stress interpolation on the displacement shape functions enables the use of low-order polynomials. In order to model beams with a large width to length ratio accurately, elongation, bending, transverse shear, non-uniform torsion (in particular constrained warping) and Wagner effects are included. The interpolation of the bimoment (the load associated with non-uniform torsion) takes into account the deformed configuration and uses hyperbolic shape functions. While this derivation yields discretized equations that are expressed in both the Hellinger–Reissner stress variables and the nodal coordinates, they are linear in the stress variables and easily reduced to a nodal coordinates-only set.

The accuracy of the proposed element stems from the interpolation of the out-of-plane bending moment: it is interpolated by a cubic polynomial, which suggests similarity to elements in a displacements-only formulation in which the displacement field is—two orders higher—a quintic polynomial.

In the literature, a large number of multibody formulations with beam-type elements are available. The following provides a sampling of the vast body of work. Some formulations are based on geometrically nonlinear beam or rod theories that describe the deformation of 1-D Cosserat continua [4, 6, 9, 27, 38, 39, 46]. Early implementations as so-called geometrically exact beam models have been detailed e.g. by Refs. [8, 18, 19, 47]. In the various corotational frameworks, implementations of beam theory can be found e.g. in work of Refs. [5, 11, 17]. The generalized strain beam formulation used in the current work can be considered a corotational approach, though formulated in absolute coordinates and without rotation interpolation issues [7, 21, 33]. Another starting point for the development of multibody beam formulations is general three-dimensional continuum mechanics theory, which has led to the absolute nodal coordinate formulation [45, 58]. For highly slender structures, geometrically nonlinear beam models based on shear-rigid beam theory have been developed [28, 57].

The use of mixed-field variational principles [2, 12, 15, 16] for the stiffness formulation of elements in multibody and finite element methods is well established in the literature. For geometrically exact beams, [40, 41] have developed several variational principles. Ref. [3] have detailed the formulation of a corotational beam element based on the Hellinger–Reissner variational principle, including the treatment of nonuniform torsion and the nonlinear Wagner stress resultant. Because the local displacements and stress resultants are interpolated linearly, it is expected to exhibit slower mesh convergence than the element of the current work.

Several formulations for the higher-order refinement of elements have been published, in particular for elements in the absolute nodal coordinate formulation [34, 44, 51, 55]. Notable is the work of Ref. [26], who also use a mixed-field approach for a refined stress interpolation that is based on the equilibrium conditions in the deformed configuration and leads to a coupling with the displacement field. Differences with the current work are that they produce the characteristic geometrically exact beam, meaning that the displacement field is a Lagrange polynomial requiring several internal nodes and therefore generally more degrees of freedom. Also, their work does not consider nonuniform torsion and Wagner effects.

In Sect. 2, an overview of the stiffness aspect of the generalized strain beam formulation is presented, so that the new element can be introduced in Sect. 3. In Sect. 4, several examples of numerical simulations are provided to demonstrate the benefits that the third-order element offers.

2 Generalized strain beam formulation

In this section, we will first formulate the discrete equations for a beam element with second-order geometrical effects. While this element has been previously introduced and implemented in the computer program Spacar [23], the derivation based on a mixed-field variational principle is a novel contribution of the current work. The benefit of this derivation is that all discrete equations stem from a single scalar energy potential, which facilitates achieving a consistent truncation across the governing equations. These second-order discrete equations are essential for deriving the third-order element in Sect. 3.

The formulation of an elastic beam element involves the discretization of a beam continuum. The governing equa-

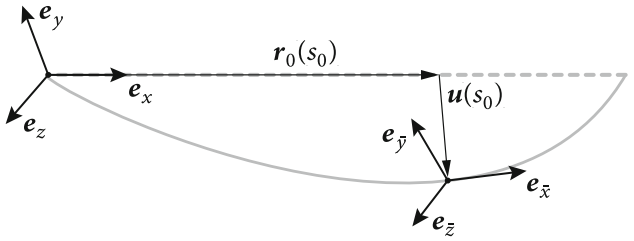

Fig. 1 Deformed beam configuration, given by the elastic line position and cross-sectional orientation. The boundary conditions are depicted as simply supported ones

tions are described first, followed by the linearized solution and the specific choices for the interpolation functions. The discretization is carried out by means of the Hu–Washizu variational principle [56], which allows for the interpolation of the displacements, as well as the strains and stresses, yielding the equilibrium, compatibility and constitutive equations.

2.1 Beam continuum

The undeformed straight reference configuration of a beam of length L is given by the position of the elastic line $\mathbf{r}_0(s)$, where $0 \leq s \leq L$ is the material coordinate. The coordinate frame is represented by the orthogonal unit vectors $\mathbf{e}_x, \mathbf{e}_y$ and $\mathbf{e}_z$. The beam is oriented such that the undeformed cross-sectional plane is normal to $\mathbf{e}_x$; the principal axes of the cross-sections are aligned with $\mathbf{e}_y$ and $\mathbf{e}_z$. Vectors and matrices in the following analysis are expressed as components in the coordinate frame represented by $\mathbf{e}_x$, $\mathbf{e}_y$ and $\mathbf{e}_z$, unless noted otherwise.

In the deformed configuration, shown in Fig. 1, the position of the elastic line is

$$\mathbf{r}(s) = \mathbf{r}_0(s) + \mathbf{u}(s) = s\mathbf{e}_x + \mathbf{u}(s), \tag{1}$$

where $\mathbf{u}$ represents the displacement. The orientation of the cross-section is represented by the orthogonal triad of unit vectors

$$\left[\mathbf{e}_{\bar{x}}\ \mathbf{e}_{\bar{y}}\ \mathbf{e}_{\bar{z}}\right] = \mathbf{R}(s)\left[\mathbf{e}_x\ \mathbf{e}_y\ \mathbf{e}_z\right], \tag{2}$$

which is rotated with respect to the undeformed configuration by rotation matrix $\mathbf{R}$. It can be parametrized in various ways. Since the deformation in this work remains limited, the rotations with respect to the undeformed configuration are small and the singularities of Euler angles pose no problems. We choose to parametrize $\mathbf{R}$ by the Euler angles according to $\mathbf{R} = \mathbf{R}_y\mathbf{R}_z\mathbf{R}_x$, where

$$\begin{aligned}
\mathbf{R}_y(s) &= \begin{bmatrix} \cos\phi_y & 0 & \sin\phi_y \\ 0 & 1 & 0 \\ -\sin\phi_y & 0 & \cos\phi_y \end{bmatrix}, \\
\mathbf{R}_z(s) &= \begin{bmatrix} \cos\phi_z & -\sin\phi_z & 0 \\ \sin\phi_z & \cos\phi_z & 0 \\ 0 & 0 & 1 \end{bmatrix}, \\
\mathbf{R}_x(s) &= \begin{bmatrix} 1 & 0 & 0 \\ 0 & \cos\phi_x & -\sin\phi_x \\ 0 & \sin\phi_x & \cos\phi_x \end{bmatrix}.
\end{aligned} \tag{3}$$

The adopted rotation order has no particular significance on the derivation in this section. The angles represent rotation with respect to and resolved in the coordinate frame denoted by $\mathbf{e}_x$, $\mathbf{e}_y$ and $\mathbf{e}_z$. For small angles, $\phi_x(s)$ is the twist angle, $\phi_y(s)$ the bending angle in the $\mathbf{e}_x, \mathbf{e}_z$-plane, and $\phi_z(s)$ the bending angle in the $\mathbf{e}_x, \mathbf{e}_y$-plane.

The curvatures $\boldsymbol{\kappa}$ and strains $\boldsymbol{\gamma}$ of the beam are given by [39]

$$\boldsymbol{\kappa}(s) = \mathbf{R}^T\mathbf{R}' = \begin{bmatrix} 0 & -\kappa_{\bar{z}} & \kappa_{\bar{y}} \\ \kappa_{\bar{z}} & 0 & -\kappa_{\bar{x}} \\ -\kappa_{\bar{y}} & \kappa_{\bar{x}} & 0 \end{bmatrix} \tag{4a}$$

and

$$\boldsymbol{\gamma}(s) = \mathbf{R}^T\left(\mathbf{e}_x + \mathbf{u}' - \mathbf{e}_{\bar{x}}\right), \tag{4b}$$

where the prime denotes differentiation with respect to s. These strain–displacement and curvature–rotation relations are collectively referred to as compatibility equations in the following sections. The components of skew-symmetric matrix $\boldsymbol{\kappa}$ are

$$\begin{aligned}
\kappa_{\bar{x}} &= \phi_x' + \phi_y' \sin\phi_z, \\
\kappa_{\bar{y}} &= \phi_y' \cos\phi_x \cos\phi_z + \phi_z' \sin\phi_x, \\
\kappa_{\bar{z}} &= \phi_z' \cos\phi_x - \phi_y' \sin\phi_x \cos\phi_z.
\end{aligned} \tag{5}$$

The warping curvature, energetically dual to the bimoment, is given by [52]

$$\kappa_w = \frac{\mathrm{d}}{\mathrm{d}s}\left(\phi_x' + \phi_y' \sin\phi_z\right). \tag{6}$$

The components of vector $\boldsymbol{\gamma}$ are

$$\begin{aligned}
\gamma_{\bar{x}}(s) &\approx u_x' - \phi_y\left(\phi_y/2 + u_z'\right) - \phi_z\left(\phi_z/2 - u_y'\right), \\
\gamma_{\bar{y}}(s) &\approx u_y' - \phi_z\left(1 + u_x'\right) + \phi_x\left(\phi_y + u_z'\right), \\
\gamma_{\bar{z}}(s) &\approx u_z' + \phi_y\left(1 + u_x'\right) + \phi_x\left(\phi_z - u_y'\right),
\end{aligned} \tag{7}$$

truncated after the second-order terms. The appropriate truncation is application-dependent and discussed in more detail in Sect. 3.3 for the new element of the current work. Axial strain $\gamma_{\bar{x}}$ can be augmented with the term

$$\frac{1}{2} I_{\mathrm{te}} \phi_x'^2, \quad \text{where } I_{\mathrm{te}} = \frac{1}{12}\left(w^2 + t^2\right), \tag{8}$$

to account for a coupling between torsion and elongation for beams with a rectangular cross-section of width w and thickness t. This term is sometimes referred to as the trapeze effect or Wagner term. It models the torsional buckling due to an axial load and the shortening of a beam that is twisted [13, 52].

The elastic energy for an initially straight beam with linear elastic material is given by

$$\begin{aligned} P_{\mathrm{elastic}} = \frac{1}{2}\int_0^L \Big[& EA\gamma_{\bar{x}}^2 + k_y GA\gamma_{\bar{y}}^2 + k_z GA\gamma_{\bar{z}}^2 \\ & + GJ\kappa_{\bar{x}}^2 + EI_y\kappa_{\bar{y}}^2 + EI_z\kappa_{\bar{z}}^2 + EI_w\kappa_w^2 \Big] \mathrm{d}s, \end{aligned} \tag{9}$$

where E is Young's modulus, A the cross-sectional area, G the shear modulus, J Saint-Venant's torsion constant, I_y and I_z the area moments of inertia about the principal axes, and I_w Vlasov's warping constant [54]. The shear correction factors k_y and k_z, as given by Ref. [10], can be used. For a rectangular cross-section, these are

$$k_y = k_z = \frac{10(1+\nu)}{12+11\nu}, \tag{10}$$

where ν is Poisson's ratio.

2.2 Linear solution

The linear solution is part of the interpolation scheme of the higher-order elements, as will be detailed in Sects. 2.3 and 3.3. It can be obtained by using the linearized compatibility relations

$$\begin{aligned} &\gamma_{\bar{x}} = u_x', \quad \gamma_{\bar{y}} = u_y' - \phi_z, \quad \gamma_{\bar{z}} = -u_z' - \phi_y, \\ &\kappa_{\bar{x}} = \phi_x', \quad \kappa_{\bar{y}} = \phi_y', \quad \kappa_{\bar{z}} = \phi_z', \quad \kappa_w = \phi_x''. \end{aligned} \tag{11}$$

The ends of the beam are referred to as node p (at $s = 0$) and node q (at $s = L$). With the simply supported boundary conditions

$$\begin{aligned} s{=}0{:}\quad & \begin{cases} u_x = 0, & \phi_x = 0, & \\ u_y = 0, & \phi_y = \phi_y^p, & \phi_x' = W^p, \\ u_z = 0, & \phi_z = \phi_z^p, & \end{cases} \\ s{=}L{:}\quad & \begin{cases} u_x = u_x^q, & \phi_x = \phi_x^q, & \\ u_y = 0, & \phi_y = \phi_y^q, & \phi_x' = W^q, \\ u_z = 0, & \phi_z = \phi_z^q, & \end{cases} \end{aligned} \tag{12}$$

eight local nodal coordinates x_l are introduced: in node p, there are the two bending angles ϕ_y^p and ϕ_z^p, and the specific twist angle W^p. In node q, there are the two bending angles ϕ_y^q and ϕ_z^q, the specific twist angle W^q, as well as the torsion angle ϕ_x^q and the axial displacement u_x^q. Other boundary conditions could have been used as well. Simply supported boundary conditions are used here, because they introduce some symmetry and make the two nodes more or less interchangeable.

The linear solution is obtained as

$$u_x = u_x^q \xi, \tag{13}$$

$$\begin{aligned} u_y = {} & L\phi_z^p\left(\xi - 2\xi^2 + \xi^3\right) + L\phi_z^q\left(-\xi^2 + \xi^3\right) \\ & + \frac{\Phi_y\left(L\phi_z^p + L\phi_z^q\right)\left(-\xi + 3\xi^2 - 2\xi^3\right)}{2 + 2\Phi_y}, \end{aligned} \tag{14}$$

$$\begin{aligned} u_z = {} & L\phi_y^p\left(-\xi + 2\xi^2 - \xi^3\right) + L\phi_y^q\left(\xi^2 - \xi^3\right) \\ & + \frac{\Phi_z\left(L\phi_y^p + L\phi_y^q\right)\left(\xi - 3\xi^2 + 2\xi^3\right)}{2 + 2\Phi_z}, \end{aligned} \tag{15}$$

$$\phi_y = -u_z' + \Phi_z\left(\phi_y^p + \phi_y^q\right)/\left(2 + 2\Phi_z\right), \tag{16}$$

$$\phi_z = u_y' + \Phi_y\left(\phi_z^p + \phi_z^q\right)/\left(2 + 2\Phi_y\right), \tag{17}$$

with dimensionless coordinate $\xi = s/L$ and dimensionless shear parameters

$$\Phi_y = \frac{12EI_z}{k_y GAL^2}, \quad \Phi_z = \frac{12EI_y}{k_z GAL^2}. \tag{18}$$

The case of bending without shear deformation can be described by setting Φ_y and Φ_z to zero.

The solution for ϕ_x contains hyperbolic functions of ξ, given in full in Appendix A. A simpler polynomial approximation, consistent with the boundary conditions, is given by

$$\begin{aligned} \phi_x = {} & \phi_x^q\left(3\xi^2 - 2\xi^3\right) + LW^p\left(\xi - 2\xi^2 + \xi^3\right) \\ & + LW^q\left(-\xi^2 + \xi^3\right) \end{aligned} \tag{19}$$

and used instead.

2.3 Second-order beam formulation

The basis for the geometrically nonlinear effects is provided by the second-order terms in the compatibility relations of Eq. (4) and given by

$$\begin{aligned} \kappa_{\bar{x}} &= \phi_x' + \phi_y'\phi_z, & \gamma_{\bar{x}} &= u_x' + u_y'^2/2 + u_z'^2/2 \\ \kappa_{\bar{y}} &= \phi_y' + \phi_z'\phi_x, & &\quad + I_{\mathrm{te}}\phi_x'^2/2, \\ \kappa_{\bar{z}} &= \phi_z' - \phi_y'\phi_x, & \gamma_{\bar{y}} &= u_y' - \phi_z, \\ & & \gamma_{\bar{z}} &= u_z' + \phi_y. \end{aligned} \tag{20}$$

The relations have been slightly simplified, because the axial stiffness and transverse shear stiffness are much larger than the bending and torsional stiffness of a beam. As a consequence, the axial displacement, u_x, and the shear strains, $\gamma_{\bar{y}}$ and $\gamma_{\bar{z}}$, are regarded as second-order effects.

The Hu–Washizu principle is used for obtaining the discretized equilibrium, compatibility and constitutive equations in terms of the displacements, strains and stresses [56]. The corresponding functional is given by

$$\begin{aligned} P_{\mathrm{HW}} &= P_{\mathrm{elastic}} \\ &+ \int_0^L \Big[F_{\bar{x}} \left(u_x' + u_y'^2/2 + u_z'^2/2 + I_{\mathrm{te}} \phi_x'^2/2 - \gamma_{\bar{x}} \right) \\ &\quad + F_{\bar{y}} \left(u_y' - \phi_z - \gamma_{\bar{y}} \right) \\ &\quad + F_{\bar{z}} \left(u_z' + \phi_y - \gamma_{\bar{z}} \right) \\ &\quad + M_{\bar{y}} \left(\phi_y' + \phi_z' \phi_x - \kappa_{\bar{y}} \right) \\ &\quad + M_{\bar{z}} \left(\phi_z' - \phi_y' \phi_x - \kappa_{\bar{z}} \right) \\ &\quad + \left(M_{\bar{x}} + B' \right) \left(\phi_x' + \phi_y' \phi_z - \kappa_{\bar{x}} \right) \\ &\quad + B \left(\phi_x'' - \kappa_w \right) \Big] \mathrm{d}s, \end{aligned} \tag{21}$$

with P_{elastic} from Eq. (9).

Besides the displacements (and rotations), this functional introduces the strains (and curvatures), and the stresses. The stresses are the beam stress resultants: the internal axial force $F_{\bar{x}}$, internal shear forces $F_{\bar{y}}$ and $F_{\bar{z}}$, internal torsion moment $M_{\bar{x}}$, internal bending moments $M_{\bar{y}}$ and $M_{\bar{z}}$, and internal bimoment B. The stress components are expressed in the moving frame denoted by $\mathbf{e}_{\bar{x}}, \mathbf{e}_{\bar{y}}, \mathbf{e}_{\bar{z}}$ in Fig. 1.

This mixed-field principle contrasts with conventional displacement-based formulations, which rely on minimization of the total potential energy (as given by Eq. (9)) and are common in finite element methods. In such formulations, there is a hierarchy between primary variables (displacements), which are discretized and solved for at the FEM nodes, and secondary variables (stresses, strains), which are derived from the primary ones. The Hu–Washizu principle allows the simultaneous discretization of all field variables for more control over the approximation accuracy.

Discretization involves the selection of sets of discrete parameters, in terms of which the displacement (and rotation), stress, and curvature (and strain) fields can then be interpolated. The resulting discretized equations are expressed in terms of those sets of discrete parameters and approximate the exact solution. The discrete stress parameters are referred to as generalized stresses; the discrete curvature and strain parameters as generalized strains.

For the interpolation of the displacements and rotations, we use the linear solution of Eqs. (13)–(17) together with Eq. (19). The local nodal coordinates x_l are the discrete parameters.

For the curvatures and strains, we construct interpolation functions by combining the linearized compatibility relations of Eq. (11) with the interpolation for the displacement and rotations of Eqs. (13)–(19), and make the specific choice to introduce eight generalized strains by carrying out the replacements

$$\begin{array}{lll} & -L\phi_y^p \to \varepsilon_3, & \\ u_x^q \to \varepsilon_1, & L\phi_y^q \to \varepsilon_4, & L^2 W^p \to \varepsilon_7, \\ L\phi_x^q \to \varepsilon_2, & -L\phi_z^p \to \varepsilon_5, & L^2 W^q \to \varepsilon_8, \\ & L\phi_z^q \to \varepsilon_6. & \end{array} \tag{22}$$

With this particular choice, we obtain strain and curvature interpolations that are constructed according to the linear beam solution, dependent only on the generalized strains ε_1 to ε_8, and given by

$$\gamma_{\bar{x}} = \varepsilon_1 / L, \tag{23}$$

$$\gamma_{\bar{y}} = \Phi_y \left(\varepsilon_5 / L - \varepsilon_6 / L \right) / \left(2 + 2\Phi_y \right), \tag{24}$$

$$\gamma_{\bar{z}} = \Phi_z \left(\varepsilon_4 / L - \varepsilon_3 / L \right) / \left(2 + 2\Phi_z \right), \tag{25}$$

$$\begin{aligned} \kappa_{\bar{x}} &= \varepsilon_2 / L^2 \left(6\xi - 6\xi^2 \right) + \varepsilon_7 / L^2 \left(1 - 4\xi + 3\xi^2 \right) \\ &\quad + \varepsilon_8 / L^2 \left(-2\xi + 3\xi^2 \right), \end{aligned} \tag{26}$$

$$\begin{aligned} \kappa_w &= \varepsilon_2 / L^3 \left(6 - 12\xi \right) \\ &\quad + \varepsilon_7 / L^3 \left(-4 + 6\xi \right) \\ &\quad + \varepsilon_8 / L^3 \left(-2 + 6\xi \right), \end{aligned} \tag{27}$$

$$\begin{aligned} \kappa_{\bar{y}} &= \varepsilon_3 / L^2 \left(4 - 6\xi \right) + \varepsilon_4 / L^2 \left(-2 + 6\xi \right) \\ &\quad + \frac{\Phi_z \left(\varepsilon_3 / L^2 - \varepsilon_4 / L^2 \right) \left(-3 + 6\xi \right)}{1 + \Phi_z}, \end{aligned} \tag{28}$$

$$\begin{aligned} \kappa_{\bar{z}} &= \varepsilon_5 / L^2 \left(4 - 6\xi \right) + \varepsilon_6 / L^2 \left(-2 + 6\xi \right) \\ &\quad + \frac{\Phi_y \left(\varepsilon_5 / L^2 - \varepsilon_6 / L^2 \right) \left(-3 + 6\xi \right)}{1 + \Phi_y}. \end{aligned} \tag{29}$$

Parameters $\boldsymbol{\varepsilon}$ have the dimension of length and can be interpreted as measures of deformation: ε_1 measures the elongation strain, ε_2, ε_7 and ε_8 nonuniform torsion (warping), ε_3 and ε_4 bending in the $\mathbf{e}_{\bar{x}}, \mathbf{e}_{\bar{z}}$-plane, and ε_5 and ε_6 bending in the $\mathbf{e}_{\bar{x}}, \mathbf{e}_{\bar{y}}$-plane.

For the interpolation of the stresses, we use eight generalized stresses σ_1 to σ_8 that are constructed specifically to be energetically dual to the generalized strains $\boldsymbol{\varepsilon}$. This means that the generalized stresses produce the virtual work $-\boldsymbol{\sigma}^T \delta\boldsymbol{\varepsilon}$. In turn, with the virtual work $\mathbf{F}^T \delta\mathbf{x}_l$ due to the applied nodal forces $\mathbf{F}$, the equilibrium condition states that

$$\boldsymbol{\sigma}^T \delta\boldsymbol{\varepsilon} = \mathbf{F}^T \delta\mathbf{x}_l \tag{30}$$

for all kinematically admissable virtual variations. Given the choice of the generalized strains $\boldsymbol{\varepsilon}$ in Eq. (22), it then follows that the generalized stresses are

$$\begin{aligned}
\sigma_1 &= F_{\bar{x}}(L), & \sigma_3 &= M_{\bar{y}}(0)/L,\\
\sigma_2 &= M_{\bar{x}}(L)/L, & \sigma_4 &= M_{\bar{y}}(L)/L,\\
\sigma_7 &= -B(0)/L^2, & \sigma_5 &= M_{\bar{z}}(0)/L,\\
\sigma_8 &= B(L)/L^2, & \sigma_6 &= M_{\bar{z}}(L)/L.
\end{aligned} \tag{31}$$

The interpolation functions for the stresses can then be constructed as

$$\begin{aligned}
F_{\bar{x}}(s) &= \sigma_1, & M_{\bar{x}}(s) &= L\sigma_2,\\
F_{\bar{y}}(s) &= \sigma_5 - \sigma_6, & M_{\bar{y}}(s) &= \sigma_3(L-s) + \sigma_4 s,\\
F_{\bar{z}}(s) &= \sigma_4 - \sigma_3, & M_{\bar{z}}(s) &= \sigma_5(L-s) + \sigma_6 s,\\
& & B(s) &= L\sigma_7(s-L) + L\sigma_8 s.
\end{aligned} \tag{32}$$

Application of the Hu–Washizu principle implies carrying out the variations with respect to the three independent fields: the displacements (and rotations), the stresses and the strains (and curvatures). By taking into account the arbitrary character of the virtual variations, three sets of equations for the unknown parameters are obtained.

Taking variations with respect to the generalized strains $\boldsymbol{\varepsilon}$ yields the constitutive equations

$$\sigma_1 = EA\varepsilon_1/L, \tag{33}$$

$$\begin{bmatrix}\sigma_2\\ \sigma_7\\ \sigma_8\end{bmatrix} = \frac{GJ}{30L^3}\begin{bmatrix}36 & -3 & -3\\ -3 & 4 & -1\\ -3 & -1 & 4\end{bmatrix}\begin{bmatrix}\varepsilon_2\\ \varepsilon_7\\ \varepsilon_8\end{bmatrix} + \frac{EI_w}{L^5}\begin{bmatrix}12 & -6 & -6\\ -6 & 4 & 2\\ -6 & 2 & 4\end{bmatrix}\begin{bmatrix}\varepsilon_2\\ \varepsilon_7\\ \varepsilon_8\end{bmatrix}, \tag{34}$$

$$\begin{bmatrix}\sigma_3\\ \sigma_4\end{bmatrix} = \frac{EI_y}{(1+\Phi_z)L^3}\begin{bmatrix}4+\Phi_z & -2+\Phi_z\\ -2+\Phi_z & 4+\Phi_z\end{bmatrix}\begin{bmatrix}\varepsilon_3\\ \varepsilon_4\end{bmatrix}, \tag{35}$$

$$\begin{bmatrix}\sigma_5\\ \sigma_6\end{bmatrix} = \frac{EI_z}{(1+\Phi_y)L^3}\begin{bmatrix}4+\Phi_y & -2+\Phi_y\\ -2+\Phi_y & 4+\Phi_y\end{bmatrix}\begin{bmatrix}\varepsilon_5\\ \varepsilon_6\end{bmatrix}, \tag{36}$$

representing the stiffness matrix of the system in terms of $\boldsymbol{\varepsilon}$ and $\boldsymbol{\sigma}$, abbreviated as $\boldsymbol{\sigma} = \mathcal{S}(\boldsymbol{\varepsilon}) = \mathbf{S}\boldsymbol{\varepsilon}$.

Taking variations with respect to the generalized stresses $\boldsymbol{\sigma}$ yields the compatibility equations

$$\begin{aligned}
\varepsilon_1 = u_x^q \quad & + L\left(2\phi_y^{p2} + 2\phi_y^{q2} + 2\phi_z^{p2} + 2\phi_z^{q2}\right)/30\\
& + L\left(-\phi_y^p\phi_y^q - \phi_z^p\phi_z^q\right)/30\\
& + I_{\mathrm{te}}\left[18\phi_x^{q2} - 3L\phi_x^q\left(W^p + W^q\right)\right]/(30L)\\
& + I_{\mathrm{te}}L^2\left(2W^{p2} - W^pW^q + 2W^{q2}\right)/30,\\
\varepsilon_2 = L\phi_x^q \quad & - L\left(\phi_y^p + \phi_y^q\right)\left(\phi_z^p - \phi_z^q\right)/2,
\end{aligned}$$

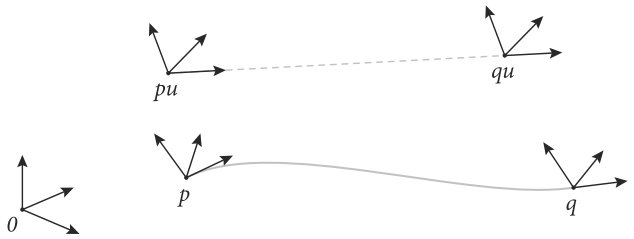

Fig. 2 Global and local coordinate frames. Nodes p and pu are depicted as separate nodes; their positions coincide

$$\begin{aligned}
\varepsilon_3 = -L\phi_y^p \quad & - L\phi_x^q\left(\phi_z^p - 2\phi_z^q\right)/10\\
& - L^2W^p\phi_z^p/10 + L^2W^q\left(\phi_z^p - \phi_z^q\right)/30,\\
\varepsilon_4 = L\phi_y^q \quad & + L\phi_x^q\left(2\phi_z^p + 9\phi_z^q\right)/10\\
& + L^2W^p\left(\phi_z^q - \phi_z^p\right)/30 - L^2W^q\phi_z^q/10,\\
\varepsilon_5 = -L\phi_z^p \quad & + L\phi_x^q\left(\phi_y^p - 2\phi_y^q\right)/10\\
& + L^2W^p\phi_y^p/10 + L^2W^q\left(\phi_y^q - \phi_y^p\right)/30,\\
\varepsilon_6 = L\phi_z^q \quad & - L\phi_x^q\left(2\phi_y^p + 9\phi_y^q\right)/10\\
& + L^2W^p\left(\phi_y^p - \phi_y^q\right)/30 + L^2W^q\phi_y^q/10,\\
\varepsilon_7 = L^2W^p \quad & - L\left(\phi_y^p + \phi_y^q\right)\left(\phi_z^p - \phi_z^q\right)/2,\\
\varepsilon_8 = L^2W^q \quad & - L\left(\phi_y^p + \phi_y^q\right)\left(\phi_z^p - \phi_z^q\right)/2,
\end{aligned} \tag{37}$$

where the terms involving shear have been ignored. These equations represent the discrete analog to the nonlinear strain and curvature relations of Eq. (20).

The two sets of discrete equations, Eqs. (33)–(36) and Eqs. (37), reflect the character of the considered beam continuum: geometrically nonlinear behavior and physically linear material behavior.

When taking variations with respect to the displacements and rotations (in the presence of some external work due to applied loads), the equilibrium equations are obtained. These are not listed here explicitly since Eq. (30) can be used directly. In Sect. 2.5, this is detailed further in the context of systems with multiple interconnected elements.

2.4 Transformation to global coordinates

In Eqs. (37), the generalized strains are expressed as functions of the displacement and rotations in a simply supported coordinate frame. For the assembly of multiple elements and the description of rigid body motion, the transformation to a global coordinate frame is necessary.

Given the unit base vectors $\mathbf{n}_x$, $\mathbf{n}_y$ and $\mathbf{n}_z$ of a global coordinate frame, the position of the two nodes with respect to the global frame is denoted by $\mathbf{r}_0^p$ and $\mathbf{r}_0^q$. The orientation of the cross-sections at the nodes with respect to the global frame is described by the rotation matrices $\mathbf{R}_0^p$ and $\mathbf{R}_0^q$, which rotate the global frame to the triad connected to the deformed cross-sections. Since the rigid body motion can be large, the

parametrization of $\mathbf{R}_0^p$ and $\mathbf{R}_0^q$ should be free from singularities. Euler parameters (unit quaternions) could be used for this purpose.

The undeformed reference configuration of the beam is indicated schematically between nodes pu and qu in Fig. 2. The local nodal coordinates have been defined with respect to this configuration (see Sect. 2.2). In this section, $\mathbf{r}_i^j$ and $\mathbf{R}_i^j$ denote the vector and rotation matrix from node i to node j. The rotational local nodal coordinates $\phi_x^q, \phi_y^p, \phi_y^q, \phi_z^p$ and ϕ_z^q are expressed in the frame attached to pu. They can be found from $\mathbf{R}_{pu}^p$ and $\mathbf{R}_{qu}^q$, which are given by $\mathbf{R}(0)$ and $\mathbf{R}(L)$, respectively, from Eq. (3).

Loop-closure type constraint equations can be used to find the relation between the local and global nodal coordinates. For the translations, the constraint equation is

$$\mathbf{r}_0^p + \mathbf{r}_p^{pu} + \mathbf{r}_{pu}^{qu} + \mathbf{r}_{qu}^q + \mathbf{r}_q^0 = \mathbf{0}. \tag{38}$$

Accounting for the simply supported boundary conditions of Eq. (12), it follows that $\mathbf{r}_p^{pu} = \mathbf{0}$ and

$$\mathbf{r}_0^p + \mathbf{R}_0^p \mathbf{R}_p^{pu} \left[L + u_x^q \; 0 \; 0\right]^T + \mathbf{r}_q^0 = \mathbf{0}. \tag{39}$$

This equation can be rearranged to

$$\left(\mathbf{R}_{pu}^p\right)^T \left[L + u_x^q \; 0 \; 0\right]^T = \left(\mathbf{R}_0^p\right)^T \left(\mathbf{r}_0^q - \mathbf{r}_0^p\right), \tag{40}$$

which expresses the relation between global nodal coordinates on the right-hand side and the local nodal coordinates $\mathbf{R}_{pu}^p$ and u_x^q on the left-hand side. From this equation, u_x^q, ϕ_y^p and ϕ_z^p can be extracted.

For the rotations, the constraint equation is

$$\mathbf{R}_0^p \mathbf{R}_p^{pu} \mathbf{R}_{pu}^{qu} \mathbf{R}_{qu}^q \mathbf{R}_q^0 = \mathbf{I}. \tag{41}$$

Since the reference configuration is straight, $\mathbf{R}_{pu}^{qu} = \mathbf{I}$. Rearranging then yields

$$\left(\mathbf{R}_{qu}^q\right)^T = \left(\mathbf{R}_0^q\right)^T \mathbf{R}_0^p \left(\mathbf{R}_{pu}^p\right)^T, \tag{42}$$

which expresses the remaining local nodal coordinates $\mathbf{R}_{qu}^q$ as functions of the known quantities on the right-hand side. From this equation, the rotations at node q, i.e. ϕ_x^q, ϕ_y^q and ϕ_z^q, can be extracted.

The warping-associated coordinates W^p and W^q are independent of the rigid body motion of the beam; no transformation is needed.

The combination of Eqs. (37) with Eqs. (40) and (42) yields

$$\boldsymbol{\varepsilon} = \mathcal{D}(\mathrm{x}). \tag{43}$$

This is the deformation function that expresses the generalized strains in terms of the global coordinate vector $\mathbf{x}$, which contains $\mathbf{r}_0^p$, $\mathbf{r}_0^q$ and the rotation parameters of $\mathbf{R}_0^p$ and $\mathbf{R}_0^q$.

2.5 Multibody systems of interconnected elements

In the generalized strain beam formulation, multibody systems are modeled by finite elements that have nodes for the connection to other elements and the interaction with the environment. An element is defined by the deformation function $\boldsymbol{\varepsilon} = \mathcal{D}(\mathrm{x})$, a constitutive model (or stress function) $\boldsymbol{\sigma} = \mathcal{S}(\boldsymbol{\varepsilon})$ and inertial properties. In the current work, an extension of the stiffness description is considered. The details of a consistent mass description for the discussed beam element can be found in Ref. [24]. Other elements, such as truss, hinge, tube and wheel elements, have been formulated [30, 43].

Elements in a system are connected by sharing nodal coordinates. The equations of motion are determined from the element deformation and stress functions, and the application of the principle of virtual work. Besides the nodal coordinates, the generalized strains can also be used as degrees of freedom, prescribed a zero value to model rigidity, a nonzero value to prescribe relative motion, or prescribed as a function of time in dynamic simulations. The equations of motion can be linearized about an arbitrary state of motion to determine buckling modes, natural modes, compliances, and state-space relations [24, 25]. A kinematic mobility analysis can be performed [1]. An arc-continuation method has been described to follow the solution path in static simulations [32].

3 Third-order stiffness formulation

In this section, the analytical nonlinear stiffness model tailored to wide and thin rectangular beams of Ref. [37] is converted to a numerical element for use in the generalized strain beam formulation.

The second-order effects, i.e. the third-order terms in the energy functional, in the previous section stem solely from the nonlinear terms in the compatibility equations. The displacement and stress interpolation is based on the linearized solution. For a description of third-order effects, i.e. fourth-order terms in the energy functional, we will make use of the knowledge of the exact beam equilibrium equations. It turns out that this way, the displacement (and rotation) interpolation based on the linear solution is still sufficiently accurate. While this is not necessarily the only way to find the fourth-order terms, it is a way that does not require a refinement of the displacement interpolation.

The continuum model based on the Hellinger–Reissner variational principle is described, along with suitable interpolation functions for the discretization. This follows the

approach of Ref. [37] with the difference that here the equations are formulated for simply supported boundary conditions instead of fixed–free ones, in order to match with the results of Sect. 2 of this paper. After that, a procedure for the numerical implementation is presented.

3.1 Hellinger–Reissner variational principle

The continuum description of the beam is based on the two-field variational principle due to Hellinger and Reissner, in which the displacements and stresses are the independent fields [56]. The derivation could also be carried out with the Hu–Washizu three-field principle, but the additional strain interpolation is an unnecessary requirement or freedom that would introduce confusing redundancy.

The Hellinger–Reissner functional can be obtained from the Hu–Washizu principle by using the constitutive equations to eliminate the strains and curvatures from Eq. (21). The variational principle then only provides the equilibrium and compatibility equations. The corresponding functional is given by

$$\begin{aligned} P_{\mathrm{HR}} = \int_0^L \Big[& \left(M_{\bar{x}} + B'\right)\kappa_{\bar{x}} + M_{\bar{y}}\kappa_{\bar{y}} + M_{\bar{z}}\kappa_{\bar{z}} \\ & + F_{\bar{x}}\gamma_{\bar{x}} + F_{\bar{y}}\gamma_{\bar{y}} + F_{\bar{z}}\gamma_{\bar{z}} + B\kappa'_{\bar{x}} \\ & - \frac{\left(M_{\bar{x}} + B'\right)^2}{2GJ} - \frac{B^2}{2EI_w} \\ & - \frac{M_{\bar{y}}^2}{2EI_y} - \frac{M_{\bar{z}}^2}{2EI_z} \\ & - \frac{F_{\bar{x}}^2}{2EA} - \frac{F_{\bar{y}}^2}{2k_yGA} - \frac{F_{\bar{z}}^2}{2k_zGA} \Big] \mathrm{d}s, \end{aligned} \tag{44}$$

where the strains $\boldsymbol{\gamma}$ and curvatures $\boldsymbol{\kappa}$ are dependent on the displacements and rotations, according to Eq. (4). The independent fields are the displacements (and rotations) and stresses.

3.2 Wagner torque

With increasing torsion angle ϕ_x, there is a nonlinear contribution to the corresponding torsion moment, given by

$$\frac{1}{360} E w^5 t \left(\phi'_x\right)^3, \tag{45}$$

that acts as a stiffening effect and starts to dominate the response. The effect is referred to as the Wagner torque [53]. Note that it is different from the torsion–elongation coupling (the trapeze or Wagner term) of Eq. (8). It is strongly dependent on the cross-sectional width and not captured by the current beam-based formulation that assumes a linear relation between the stress resultants and the measures of beam deformation of Eq. (4). The Wagner torque can be incorporated by including the associated strain energy per unit length [31]

$$\frac{1}{1440} E w^5 t \kappa_{\bar{x}}^4 \tag{46}$$

in the integrand of P_{HR}.

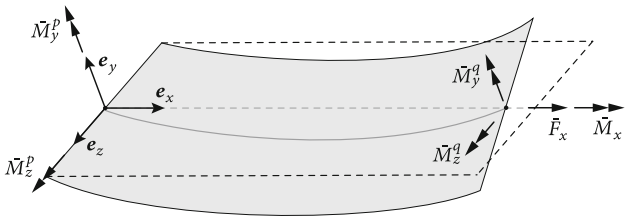

Fig. 3 Deformed configuration of a wide and thin beam, depicted with the simply supported boundary conditions of Eq. (12). The nodal loads are expressed in the fixed frame $\mathbf{e}_x$, $\mathbf{e}_y$, $\mathbf{e}_z$

3.3 Interpolation

Considering Fig. 3, the exact equilibrium equations for a finite beam segment are given by

$$\begin{aligned} \begin{bmatrix} M_{\bar{x}}(s) \\ M_{\bar{y}}(s) \\ M_{\bar{z}}(s) \end{bmatrix} &= \mathbf{R}(s)^T \left\{ [\mathbf{r}(L) - \mathbf{r}(s)] \times \mathrm{F}_{\mathrm{appl.}} \right\} \\ &\quad + \mathbf{R}(s)^T \begin{bmatrix} \bar{M}_x \\ \bar{M}_y^q \\ \bar{M}_z^q \end{bmatrix}, \end{aligned} \tag{47}$$

where

$$\mathbf{F}_{\mathrm{appl.}} = \begin{bmatrix} \bar{F}_x \\ -\left(\bar{M}_z^p + \bar{M}_z^q\right)/(L + u_x^q) \\ \left(\bar{M}_y^p + \bar{M}_y^q\right)/(L + u_x^q) \end{bmatrix}. \tag{48}$$

This expression holds between the internal moments $M_{\bar{x}}$, $M_{\bar{y}}$, $M_{\bar{z}}$ expressed in moving frame $\mathbf{e}_{\bar{x}}$, $\mathbf{e}_{\bar{y}}$, $\mathbf{e}_{\bar{z}}$ at s, and some externally applied loads $\bar{F}_x$, $\bar{M}_x$, $\bar{M}_y^p$, $\bar{M}_y^q$, $\bar{M}_z^p$, $\bar{M}_z^q$ at $s = 0$ and $s = L$, expressed in the fixed frame $\mathbf{e}_x$, $\mathbf{e}_y$, $\mathbf{e}_z$. The linearized solution, i.e. equilibrium in the undeformed configuration, is obtained when $\mathbf{R}$ is reduced to the identity matrix, and $\mathbf{u} = \mathbf{0}$ so that $\mathbf{r} = \mathbf{r}_0$.

The purpose of the element is to model sheet flexures with the distinct dimensions as they are often encountered in precision flexure mechanism. We make the specific assumptions that

- the width is the same order of magnitude as the length,
- the transverse displacement along the thickness dimension less than 15% of the length, and

- the failure strain of the material is of the order of 0.003, which is a realistic failure strain for high tensile strength metals.

Also, all loads remain sufficiently low that no failure due to buckling or plasticity occurs. These assumptions can be used to estimate the magnitude of the various nonlinear terms in the compatibility equations of Eq. (4) and the equilibrium equations of Eq. (47), in turn providing magnitude estimates for the terms in the energy functional of Eq. (44) and the rationale for the truncation of terms such that only the significant terms up to the fourth order are retained.

We have estimated that the thickness is two orders of magnitude smaller than the length [37]. With the width dimension along the z-axis, $\kappa_{\bar{y}}$ is estimated to be two orders smaller than $\kappa_{\bar{x}}$ and $\kappa_{\bar{z}}$. Also, u_y is estimated to be two orders larger than u_x and u_z, and ϕ_y to be two orders smaller than ϕ_x and ϕ_z. Furthermore, it follows that the leading order terms in the energy functional, including the fourth-order ones, are retained when the exact equilibrium equations of Eq. (47) are reduced to

$$\begin{aligned} M_{\bar{x}}(s) &= \widetilde{M}_x + u_y(s)\left(\widetilde{M}_y^p + \widetilde{M}_y^q\right)/L \\ &\quad + u_y'(s)\left[\widetilde{M}_y^p\,(\xi-1) + \widetilde{M}_y^q\,\xi\right], \\ M_{\bar{y}}(s) &= \widetilde{M}_y^p\,(\xi-1) + \widetilde{M}_y^q\,\xi, \\ M_{\bar{z}}(s) &= \widetilde{M}_z^p\,(\xi-1) + \widetilde{M}_z^q\,\xi \\ &\quad + u_y(s)\widetilde{F}_x - \phi_x(s)\left[\widetilde{M}_y^p\,(\xi-1) + \widetilde{M}_y^q\,\xi\right], \end{aligned} \tag{49}$$

and the exact compatibility equations of Eq. (4) are reduced to

$$\begin{aligned} \kappa_{\bar{x}} &= \phi_x', & \gamma_{\bar{x}} &= u_x' + u_y'^2/2, \\ \kappa_{\bar{y}} &= \phi_y' + \phi_x\phi_z' & \gamma_{\bar{y}} &= 0, \\ &\approx \phi_y' + \phi_x u_y'', & \gamma_{\bar{z}} &= u_z' + \phi_y. \\ \kappa_{\bar{z}} &= \phi_z' \approx u_y'', \end{aligned} \tag{50}$$

Here, $\xi = s/L$ and the transverse shear along the thickness dimension $\gamma_{\bar{y}}$ is ignored so $\phi_z = u_y'$. In Eq. (49), the six unknown Hellinger–Reissner stress variables $\widetilde{M}_x$, $\widetilde{M}_y^p$, $\widetilde{M}_y^q$, $\widetilde{M}_z^p$, $\widetilde{M}_z^q$ and $\widetilde{F}_x$, denoted by a superscript tilde, have been introduced. Displacement $u_y(s)$ and rotation $\phi_x(s)$ are interpolated according to the linear solution Eqs. (13)–(19), disregarding the effect of shear deformation on $u_y(s)$.

For a bimoment interpolation that is consistent with the torsion interpolation $M_{\bar{x}}$ of Eq. (49), and which takes the deformed configuration into account, the differential equation

$$\begin{aligned} GJ\kappa_{\bar{x}} - EI_w\kappa_{\bar{x}}'' &= M_{\bar{x}}(s), \\ \kappa_{\bar{x}}(0) &= W^p, \\ \kappa_{\bar{x}}(L) &= W^q \end{aligned} \tag{51}$$

can be used to calculate first $\kappa_{\bar{x}}(s)$ and then the bimoment $B(s) = EI_w\kappa_{\bar{x}}'(s)$. The bimoment interpolation obtained this way contains hyperbolic functions of s and is dependent on the unknown Hellinger–Reissner stress variables $\widetilde{M}_x$, $\widetilde{M}_y^p$, $\widetilde{M}_y^q$, the nodal coordinates ϕ_x^q, ϕ_z^p, ϕ_z^q, W^p, W^q, and the dimensionless parameter $\lambda = L\sqrt{GJ/(EI_w)}$. It is given in full in Appendix B.

The assumption of having only one small dimension is reflected in Eqs. (49) and (50): since the axial stiffness and the in-plane bending stiffness for this type of beam are much larger than the torsional stiffness and the out-of-plane bending stiffness, only the nonlinear terms in the elongation strain $\gamma_{\bar{x}}$ and in-plane curvature $\kappa_{\bar{y}}$ are needed. Also, the deformed-configuration equilibrium terms are only needed for the torsion moment $M_{\bar{x}}$ and the out-of-plane bending moment $M_{\bar{z}}$. These terms in the expressions for $M_{\bar{x}}$ and $M_{\bar{z}}$ constitute the third-order effects of the current work.

With the stress interpolation functions of Eq. (49), the compatibility equations of Eq. (50), and the displacement and rotation interpolation simply according to the linear solution of Eqs. (13)–(19), the Hellinger–Reissner functional of Eq. (44) can be expressed in terms of the six stresses $\widetilde{F}_x$, $\widetilde{M}_x$, $\widetilde{M}_y^p$, $\widetilde{M}_y^q$, $\widetilde{M}_z^p$, $\widetilde{M}_z^q$ and the nodal coordinates u_x^q, ϕ_x^q, ϕ_y^p, ϕ_y^q, ϕ_z^p, ϕ_z^q and W^p, W^q.

Taking variations with respect to the nodal coordinates yields the discretized equilibrium equations; taking variations with respect to the stresses yields the discretized constitutive equations. An important observation is the fact that the exact equilibrium equation of Eq. (47) is linear in the applied loads and the energy functional of Eq. (44) is at most quadratic in the stresses. As a consequence, the variations with respect to the stresses are always linear in the stresses whenever some form of the equilibrium equation of Eq. (47) is used. Hence, the stress variables can always be solved for and eliminated, yielding in turn a standard displacements-only based discretization.

3.4 Initial deformation

The Hellinger–Reissner functional in Eq. (44) assumes that the beam is straight in its undeformed, stress-free configuration. The effect of initial curvature and initial strain can be included by adding the terms

$$\begin{aligned} -\int_0^L \big[&\left(M_{\bar{x}} + B'\right)\kappa_{\bar{x},0} + M_{\bar{y}}\kappa_{\bar{y},0} + M_{\bar{z},0}\kappa_{\bar{z},0} \\ &+ F_{\bar{x}}\gamma_{\bar{x},0} + F_{\bar{y},0}\gamma_{\bar{y},0} + F_{\bar{z}}\gamma_{\bar{z},0} + B\kappa_{\bar{x},0}'\big]\,\mathrm{d}s \end{aligned} \tag{52}$$

to P_{HR}. The subscript 0 denotes the value of the initial strain and curvature. In the current formulation, deformations in and out of the plane of the beam are treated differently: out-of-plane deformations are assumed to be much larger, requiring fourth-order energy terms, while in-plane defor-

mations can be described with lower-order terms. Therefore, adding Eq. (52) is appropriate for large initial out-of-plane deformations (related to $\kappa_{\bar{x}}$ and $\kappa_{\bar{z}}$) but only for small initial in-plane deformations (related to $\kappa_{\bar{y}}$, $\gamma_{\bar{x}}$ and $\gamma_{\bar{z}}$), consistent with the assumptions of Eqs. (49)–(50). For larger initial in-plane deformations, Eqs. (49)–(50) and the interpolation functions would need to be revised. For a second-order beam element in the generalized strain beam formulation with initial deformation, see Ref. [30].

3.5 Closed-form solution

It has been shown that the internal energy P_{HR} of Eq. (44) with the interpolation functions from Sect. 3.3 can also be used to develop an analytical parametric model for sheet flexures [37]. Such a model can be useful in a design context as it offers parametric insight.

This model can be obtained by combining the internal energy P_{HR} with some external work due to applied loads at the nodes, such as

$$\bar{F}_x u_x^q + \bar{M}_x \phi_x^q + \bar{M}_y^p \phi_y^p + \bar{M}_y^q \phi_y^q + \bar{M}_z^p \phi_z^p + \bar{M}_z^q \phi_z^q. \quad (53)$$

Note that the superscript bars denote the loads applied at the nodes. Superscript tildes, introduced earlier, denote the unknown Hellinger–Reissner stress variables. The variations of the total energy expression yield a nonlinear system of equations that happens to admit a closed-form polynomial solution when, first, the six Hellinger–Reissner stresses are eliminated and, second, the remaining smaller variables are expressed as functions of the larger variables, as

$$\begin{aligned}&\left[u_x^q, \phi_y^p, \phi_y^q, \bar{M}_x, \bar{M}_z^p, \bar{M}_z^q\right]^T = \\ &\quad \mathbf{f}\left(\phi_x^q, \phi_z^p, \phi_z^q, \bar{F}_x, \bar{M}_y^p, \bar{M}_y^q\right).\end{aligned} \quad (54)$$

Variables u_x^q, ϕ_y^p, ϕ_y^q are small because they correspond with motion in the directions of relatively high stiffness; variables $\bar{M}_x$, $\bar{M}_z^p$, $\bar{M}_z^q$ are small because they correspond with loads in the directions of relatively low stiffness. The opposite holds for the right-hand side variables. This solution can be found in closed form, precisely because the interpolation is based on the assumption that there is (only) one small dimension. This leads to a nonlinear coupling between only certain variables.

When transformed to cantilever boundary conditions, the analytical solution in this particular format provides a parametric nonlinear model for the effects due to the geometric stiffness as encountered in e.g. flexure mechanisms in precision manipulation [37]. The closed-form solution of Eq. (54) is used in part in Sect. 3.6 as well.

3.6 Numerical implementation

Numerical elements in the generalized strain beam formulation are defined by the deformation function $\boldsymbol{\varepsilon} = \mathcal{D}(\mathrm{x})$ and the stress function $\boldsymbol{\sigma} = \mathcal{S}(\boldsymbol{\varepsilon})$. The equilibrium equations are formulated in terms of the deformation function. For the second-order beam element in Sect. 2, we have shown that both functions can be obtained as the discretized compatibility and constitutive equations of a beam continuum. The third-order effects of this section stem from the consideration of the deformed-configuration equilibrium in combination with nonlinear compatibility equations. To account for these effects in the generalized strain beam formulation, we choose to use a refinement of the stress function $\mathcal{S}(\boldsymbol{\varepsilon})$ and use the same deformation function $\mathcal{D}(\mathbf{x})$ as for the second-order element. It means that the third-order effects are accounted for solely by a nonlinear constitutive relation, which facilitates the numerical implementation.

To derive the appropriate constitutive relation, we observe that the variation of the potential energy with respect to the generalized strains is equal to the negative virtual work produced by the generalized stresses, i.e.

$$\delta P = \frac{\partial P}{\partial \varepsilon_i}\delta\varepsilon_i = \sigma_i \delta\varepsilon_i, \quad (55)$$

so that the generalized stresses can be found as

$$\sigma_i = \frac{\partial P}{\partial \varepsilon_i}. \quad (56)$$

This relation cannot be used directly with P_{HR}, since P_{HR} is a function of six Hellinger–Reissner stress variables and the local nodal coordinates $\mathbf{x}_l$, i.e.

$$\begin{aligned}P_{\text{HR}} = f_1\Big(&\widetilde{F}_x, \widetilde{M}_x, \widetilde{M}_y^p, \widetilde{M}_y^q, \widetilde{M}_z^p, \widetilde{M}_z^q, \\ &u_x^q, \phi_x^q, \phi_y^p, \phi_y^q, \phi_z^p, \phi_z^q, W^p, W^q\Big),\end{aligned} \quad (57)$$

and only indirectly dependent on $\boldsymbol{\varepsilon}$ through Eqs. (37). Since the $\boldsymbol{\varepsilon}$ are considered to be small quantities, a partial inversion of Eqs. (37),

$$u_x^q \approx \varepsilon_1 - \left(2\varepsilon_5^2 + \varepsilon_5\varepsilon_6 + 2\varepsilon_6^2\right)/(30L), \quad (58)$$

$$\phi_x^q \approx \varepsilon_2/L, \quad (59)$$

$$\begin{aligned}\phi_y^p \approx\ &-\varepsilon_3/L + \varepsilon_2\left(\varepsilon_5 + 2\varepsilon_6\right)/(10L^2) \\ &+ \varepsilon_7\varepsilon_5/(10L^2) \\ &- \varepsilon_8\left(\varepsilon_5 + \varepsilon_6\right)/(30L^2),\end{aligned} \quad (60)$$

$$\begin{aligned}\phi_y^q \approx\ &\varepsilon_4/L + \varepsilon_2\left(2\varepsilon_5 - 9\varepsilon_6\right)/(10L^2) \\ &+ \varepsilon_8\varepsilon_6/(10L^2) \\ &- \varepsilon_7\left(\varepsilon_5 + \varepsilon_6\right)/(30L^2),\end{aligned} \quad (61)$$

$$\phi_z^p \approx -\varepsilon_5/L, \quad (62)$$

$$\phi_z^q \approx \varepsilon_6/L, \tag{63}$$

$$W^p \approx \varepsilon_7/L^2, \tag{64}$$

$$W^q \approx \varepsilon_8/L^2, \tag{65}$$

can be used to replace the local nodal coordinates with ε_1 to ε_8. Given that the fourth-order terms in P_{HR} are at most quadratic in the local nodal coordinates, Eqs. (58)–(65) can be truncated after the second-order terms in $\boldsymbol{\varepsilon}$. Since the axial and in-plane deformation are much smaller than the torsion and out-of-plane deformation, ε_1, ε_3, ε_4 may be regarded as second-order terms. By taking the variations with respect to the six stress parameters in P_{HR}, the linear equations

$$\mathbf{b}_1 = \left[\mathbf{A}_1\left(\mathbf{x}_l\right)\right]\left[\widetilde{F}_x, \widetilde{M}_x, \widetilde{M}_y^p, \widetilde{M}_y^q, \widetilde{M}_z^p, \widetilde{M}_z^q\right]^T \tag{66}$$

are obtained, where matrix $\mathbf{A}_1$ is a function of $\mathbf{x}_l$. While it may seem tempting to eliminate all six stress parameters from P_{HR} analytically, the energy expression then turns into a very large rational function and becomes cumbersome to deal with (even with analytical solver software), especially when the derivatives (see Eq. (56)) are calculated. Once more, the consequences of the assumption that there is (only) one small dimension can be exploited, in a similar fashion to the closed-form solution of Sect. 3.5. Equation (66) can be solved for the specific combination of the small nodal coordinates u_x^q, ϕ_y^p, ϕ_y^q, associated with high axial and in-plane bending stiffness, and the loads $\widetilde{M}_x$, $\widetilde{M}_z^p$, $\widetilde{M}_z^q$, associated with the low torsion and out-of-plane bending stiffness. The resulting expression then remains a simple polynomial, similar to Eq. (54). This polynomial can be used to reduce Eqs. (57) and (66) to

$$\mathbf{b}_2 = \left[\mathbf{A}_2\left(\boldsymbol{\varepsilon}\right)\right]\left[\widetilde{M}_y^p\ \widetilde{M}_y^q\ \widetilde{F}_x\right]^T, \tag{67}$$

$$P_{\mathrm{HR}} = f_2\left(\widetilde{M}_y^p, \widetilde{M}_y^q, \widetilde{F}_x, \boldsymbol{\varepsilon}\right), \tag{68}$$

where the partially inverted deformation functions, given by Eqs. (58)–(65), have been used to replace $\mathbf{x}_l$ in f_1 and $\mathbf{A}_1$ with $\boldsymbol{\varepsilon}$.

The energy potential is now a function of $\boldsymbol{\varepsilon}$ and the three stress variables $\widetilde{M}_y^p$, $\widetilde{M}_y^q$ and $\widetilde{F}_x$. Expressions for the refined generalized stresses $\boldsymbol{\sigma}$ are obtained by calculating the derivatives of P_{HR} (see Eq. (56)) and using the chain rule for the dependency of the stress variables on $\boldsymbol{\varepsilon}$ according to Eq. (67), yielding

$$\boldsymbol{\sigma} = \mathcal{S}\left(\boldsymbol{\varepsilon}, \widetilde{M}_y^p, \widetilde{M}_y^q, \widetilde{F}_x, \frac{\partial \widetilde{M}_y^p}{\partial \boldsymbol{\varepsilon}}, \frac{\partial \widetilde{M}_y^q}{\partial \boldsymbol{\varepsilon}}, \frac{\partial \widetilde{F}_x}{\partial \boldsymbol{\varepsilon}}\right). \tag{69}$$

This refined stress function can be used to account for the third-order effects that were derived in this section. The vector function is a polynomial of manageable size that still depends on three of the Hellinger–Reissner stress variables and their derivatives with respect to the generalized strains. For the numerical evaluation of $\boldsymbol{\sigma}$ for a given $\boldsymbol{\varepsilon}$, the 3-by-3 linear system of Eq. (67) can be solved numerically for $\widetilde{M}_y^p$, $\widetilde{M}_y^q$ and $\widetilde{F}_x$. Their derivatives in turn can be solved numerically from the linear equations

$$\left[\mathbf{A}_2\left(\boldsymbol{\varepsilon}\right)\right]\begin{bmatrix}\partial \widetilde{M}_y^p/\partial\varepsilon_i \\ \partial \widetilde{M}_y^q/\partial\varepsilon_i \\ \partial \widetilde{F}_x/\partial\varepsilon_i\end{bmatrix} = \mathbf{b}_2 - \left[\partial \mathbf{A}_2/\partial\varepsilon_i\right]\begin{bmatrix}\widetilde{M}_y^p \\ \widetilde{M}_y^q \\ \widetilde{F}_x\end{bmatrix}, \tag{70}$$

for $i = 1, \ldots, 8$. These equations are obtained by differentiating the left- and right-hand side Eq. (67) with respect to ε_i. Since the eight linear systems contain the same $\mathbf{A}_2$, its decomposition can be reused for faster numerical evaluation.

4 Application examples

The beam element with third-order stiffness effects has been incorporated into the Spacar multibody software program [23]. In this section, a comparison with the earlier second-order beam element [22], summarized in Sect. 2.3, is carried out for static simulations. The examples are based on flexure mechanisms that are used in precision manipulation; these mechanisms commonly consist of sheet flexures (also referred to as leaf springs or flexure strips), which are wide and thin rectangular beams.

As this work concerns an extended stiffness description, the static equilibrium in deformed configurations is studied. In Spacar, the algorithm described by Ref. [32] is used for obtaining static solutions. Here, the residual vector on the system level is a nonlinear function of the global coordinates $\mathbf{x}$, the generalized strains $\boldsymbol{\varepsilon}$ and the generalized stresses $\boldsymbol{\sigma}$. The final deformed configuration is reached by prescribing a displacement or a rotation in successive load steps, at each of which the unknown x, $\boldsymbol{\varepsilon}$ and $\boldsymbol{\sigma}$ are simultaneously solved for by Newton–Raphson iteration, using a direct solver with Gaussian elimination and partial pivoting. The iteration is stopped when the relative L^1-norm of the corrections is less than $5 \cdot 10^{-7}$.

For the comparisons in this section, a single-core Fortran-based standard dense linear algebra implementation of the program is used, running on a Mac mini with 3 GHz Intel Core i5 processor and 32 GB DDR4 RAM on macOS 14.5. It is noted that Spacar is a software program for flexible multibody dynamics simulations of a general class of systems, and therefore not specifically optimized for just statics simulations of systems with many components. Though the focus of the present work is on algorithmic improvements, there are hardware and computational resource optimizations with the potential for speed improvements (also see Sect. 4.3).

As a reference solution, the ANSYS beam element BEAM188 and plate (shell) element SHELL181 are used.

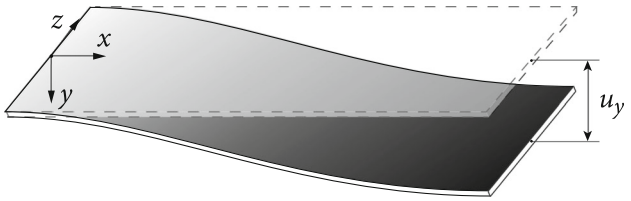

Fig. 4 Cantilever beam, deflected due to a prescribed displacement u_y. The rotation about the z-axis at the free end is fixed to a zero value. The depicted width-to-length ratio is smaller than simulated

The beam element has 2 external nodes with 7 degrees of freedom each (translations, rotations and warping). It uses Timoshenko beam theory, supports constrained warping of cross-sections following [42], and includes stress-stiffness terms for flexural, lateral and torsional buckling effects. The element uses two additional internal nodes, cubic shape functions for all displacements and rotations, and three integration points along the length. The plate element has 4 nodes with 6 degrees of freedom each (translations and rotations) and captures both the membrane and bending stiffness. It uses 2×2 in-plane integration points and 3 through-thickness integration points. The full integration option with incompatible modes [48] is used for the higher accuracy over the reduced integration option.

4.1 Cantilever beam

Consider the sheet flexure in Fig. 4, represented by the cantilever beam with dimensions 100 mm, 100 mm and 2.25 mm, Young's modulus 200 GPa and Poisson's ratio 0.3. The displacement in y-direction at the free end is prescribed a value up to 15% of the length, which is reached in 15 load steps. The rotation about the z-axis at the free end is fixed to a zero value. In the deflected equilibrium configuration, the prescribed displacement and rotation are removed and equivalent forces and moments at the free end are applied. The linearized equilibrium equations are then used to calculate the compliance matrix. Figure 5 shows the diagonal components for the translational x- and z-direction. It can be seen that more than three Spacar elements with the conventional second-order stiffness formulation are needed for reasonable convergence. The geometrically nonlinear BEAM188 beam element in ANSYS performs similar to the Spacar element for the x-component of the compliance; for the z-component, the ANSYS one-element result is closer to the Spacar three-element result. A single element with the third-order stiffness formulation of the current work performs better and lies already within 0.8% of the converged value, represented by the 20-element Spacar and ANSYS solutions, at maximum deflection. Convergence of the ANSYS beam element is rapid, since the 2-element solution is within 0.7% for the x-component and 0.2% for the z-component of the 20-element ANSYS solution.

It is noted that for a larger deflection of $u_y/L = 0.5$, the results are qualitatively the same: the quantitative results for $\partial u_z/\partial F_z$ show that the single third-order element is within 2.4% of the 20-element ANSYS solution, whereas the 1-element ANSYS model is 19.9% off, requiring the 2-element solution to be within 1% of the converged solution.

The contribution of the Wagner torque to the torsion moment is relatively straightforward and summarized in Sect. 3.2. It can also have a significant effect on various components of the compliance matrix computed in a deformed state. This is illustrated by the same sheet flexure of Fig. 4 but with a different loading condition at the free end: transverse displacement u_y is set to $0.15L$; now, also z-axis rotation ϕ_z is set to 0.15 radians and the x-axis twist angle ϕ_x is incremented from 0 up to a value of 0.15 radians. In similar fashion as before, the compliance matrix at the free end is calculated. Models with the third-order element are compared to an ANSYS model with sufficient nonlinear SHELL181 elements for convergence. These plate elements are used to model the Wagner torque, which the ANSYS BEAM181 element does not take into account. It can be seen that the Spacar models with the third-order beam elements converge to the ANSYS solution. At least three elements are needed to reduce the deviation to 2.4% at the maximum twist angle. When the Wagner torque term is excluded from the element formulation, it can be seen that the deviation increases to 38%, showing the significance of the term on component $\partial u_x/\partial M_y$ of the compliance matrix. Similar observations hold for the other compliance matrix components. With three third-order beam elements, the deviation of all components is at most 6.4% when the Wagner torque is accounted for.

It is noted that this load case requires multiple third-order elements in order to model the Wagner torque accurately, unlike the previous load case, in which a single third-order element suffices. This can be explained by the refined moment interpolation used for the element: the Hellinger–Reissner moment interpolation accounts for an approximate deformed configuration of the sheet flexure (as evidenced by the presence of $u_y(s)$ and $\phi_x(s)$ in Eq. (49)) to enable the use of fewer elements. This approximation does not include the Wagner torque, though, because the relationship is nonlinear and nontrivial.

While the goal of the proposed element is to avoid the slower computation with plate elements whenever possible, there are several load cases that may require the higher accuracy of plate elements. Besides the obvious limitation that the beam element only has an interface at two of its four sides, the effects of anticlastic curvature are not captured. As an example, even without deformation, for a straight beam, the deviation in the stiffness coefficients $\partial F_y/\partial u_y$, $\partial F_y/\partial \phi_z$ and $\partial M_z/\partial \phi_z$ evaluated at the free end of the cantilever beam

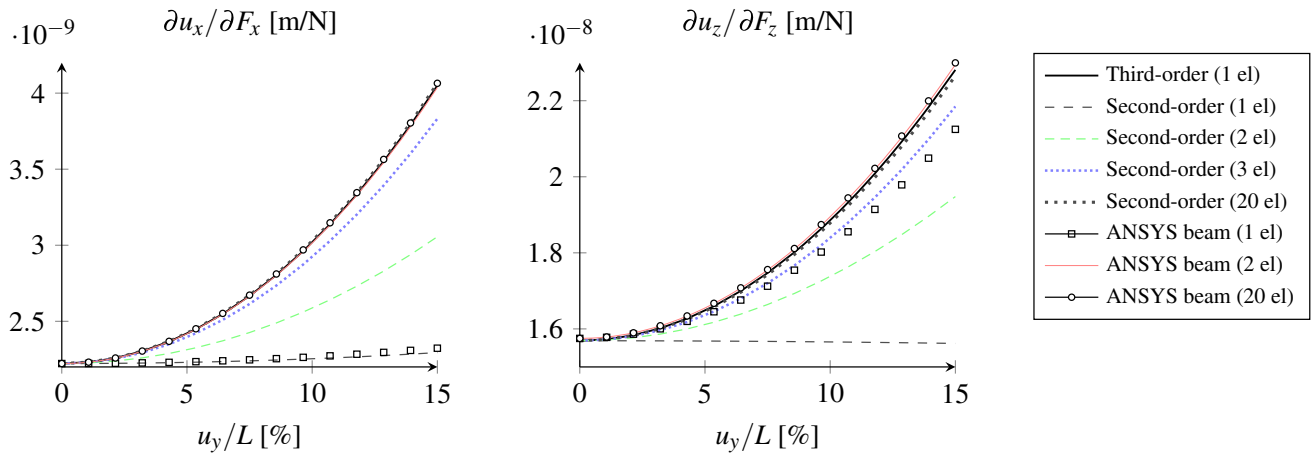

Fig. 5 Two diagonal components of the compliance matrix at the free end of a cantilever beam with increasing deflection. Graphs show the new third-order element in Spacar, the second-order element in Spacar and the ANSYS BEAM188 element

Table 1 Parameters of the two sheet flexures that make up a single folded sheet flexure in the spherical flexure joint model. Parameters ψ, r and θ_1 are defined in Fig. 7 of Ref. [35]

Length	68.1 mm
Width	28.2 mm
Thickness	0.838 mm
Young's modulus E	210 GPa
Poisson's ratio ν	0.30
Fold angle ψ	86.2 deg
Center distance r	34.3 mm
Azimuth θ_1	40.2 deg

in Fig. 4 is 7.8% when comparing the third-order beam element with the SHELL181 plate element reference solution [37]. The deviation stems from the effect of local anticlastic curvature constraints at the two beam ends, manifests itself even for infinitesimal deformation, and depends on the width to length ratio. Additionally, the other facet of anticlastic curvature, i.e. a bending stiffness that increases with deformation, is not captured either by the beam formulation. In the limit case of plane strain, it causes a stiffness increase of $1/(1-\nu^2)$.

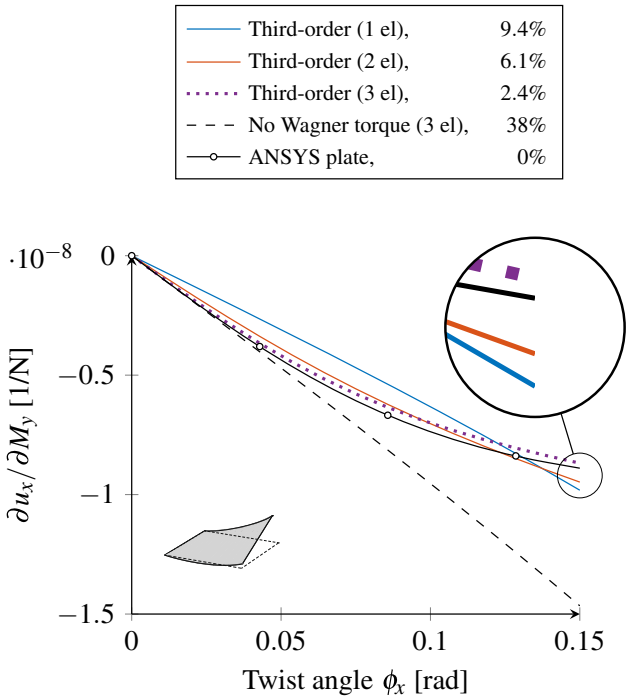

Fig. 6 Effect of the Wagner torque nonlinearity on a compliance matrix component. Comparison of Spacar solutions with the third-order beam element and a converged ANSYS solution with nonlinear SHELL181 plate elements. The legend summarizes the relative deviation in percent at $\phi_x = 0.15$ radians with respect to the ANSYS solution

4.2 Spherical flexure joint

Consider the flexible mechanism in Fig. 7 as described by Naves et al. [35]. It consists of two sets of three so-called folded sheet flexures (also referred to as folded leaf springs). One set is connected between the fixed base and a rigid intermediate body; the other set between the rigid intermediate body and a rigid end-effector. Each folded sheet flexure can be regarded as two regular sheet flexures, i.e. as two wide and thin rectangular beams, connected at an angle, with dimensions according to Table 1. The folded sheet flexures are positioned such that the six fold lines all intersect the same point. This ensures that the mechanism has behavior that is approximately kinematically equivalent to a spherical joint, i.e. the end-effector has three rotational degrees of freedom with respect to the fixed base. Since this flexible embodiment of a spherical joint consists of elastically deforming components, the approximation of that behavior means that the rotations of the end-effector are associated with rela-

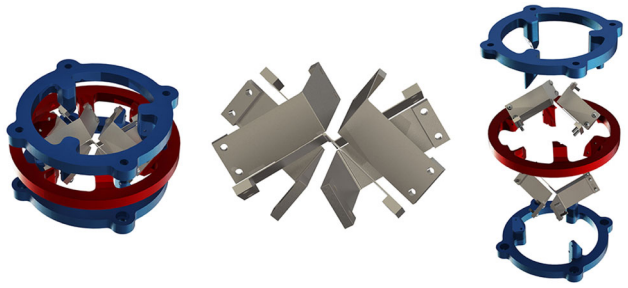

Fig. 7 Spherical flexure joint [35]. Center figure shows the six folded sheet flexures without the frames. Right figure shows an exploded view. Design parameter details can be found in Ref. [35]

	Normalized comp. time	Maximum supp. stiffn.
Third-order (1 el)	1.0	9.77
Third-order (2 el)	3.3	9.61
Second-order (1 el)	0.9	10.95
Second-order (2 el)	3.1	9.68
Second-order (4 el)	9.6	9.63
ANSYS plate	-	9.81

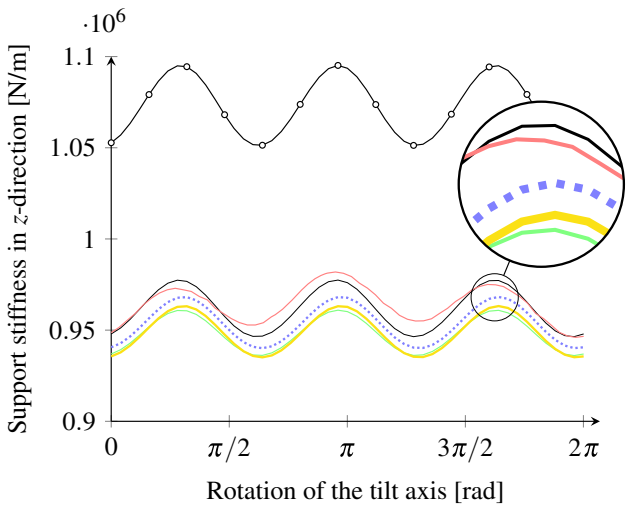

Fig. 8 Support stiffness of the spherical flexure joint from models with the second-order and third-order beam element in Spacar. The legend summarizes the computation time (second column) and the maximum of the support stiffness in 10^5N/m (third column). The computation times are normalized with respect to the third-order 1-element model, which takes 2.45 s

tively low stiffness compared to the translations. The high stiffness components are referred to as support stiffness components. The change in support stiffness that accompanies deformation in the directions of low stiffness is an important performance characteristic, since it tends to limit the motion-guiding and load-carrying ability. It is governed by the geometric stiffness.

This system is simulated by 1, 2 and 4 beam elements per sheet flexure, i.e. 2, 4 and 8 elements per folded sheet flexure. Figure 8 shows the support stiffness in z-direction at the center of the end-effector when the end-effector is tilted

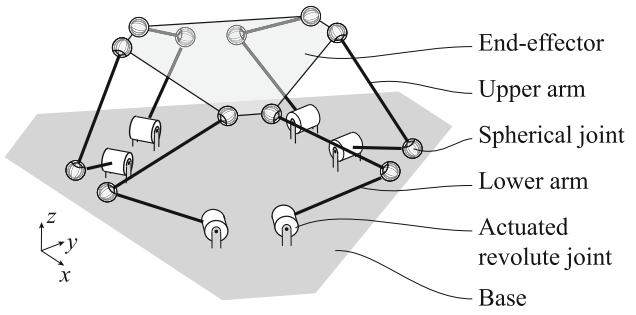

Fig. 9 Schematic overview of the flexure-based hexapod. The spherical flexure joints contain the flexible elements: each of the twelve spherical flexure joints consists of six folded sheet flexures

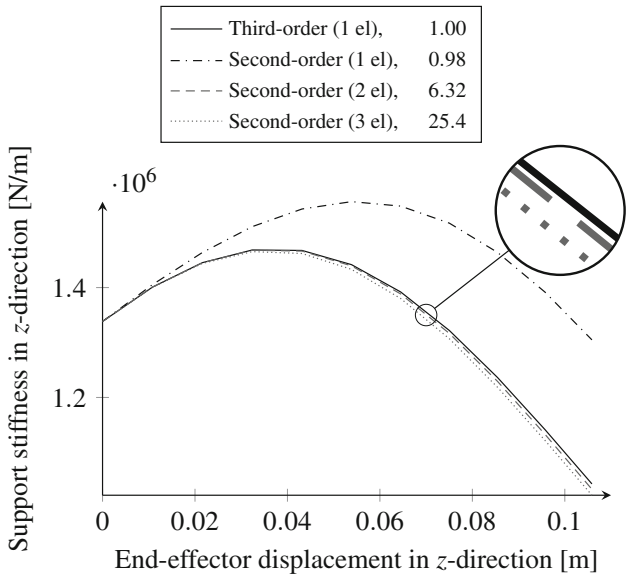

Fig. 10 Computation time for various element types in modeling the support stiffness of the flexure-based hexapod. Legend shows computation time, normalized with respect to the third-order 1-element model, which takes 122 s

15 degrees with respect to an axis in the x, y-plane. That tilt axis is rotated 2π radians about the z-axis in 50 steps. The legend shows the computation times. It can be seen that a single third-order element is already very close to the solution of four second-order elements: the difference in peak stiffness is only 1.5%. While computations with the third-order element itself are a little bit slower, the comparison with the two-element second-order solution of similar performance shows a reduction of 68% in computation time.

4.3 Flexure-based hexapod

A larger multibody simulation comes from a model of the fully flexure-based T-Flex hexapod [36], as shown in Fig. 9. The hexapod consists of six actuated legs that each have two links, two spherical flexure joints and one revolute joint at the base. This means that the model has twelve spherical flexure joints that each consist of six folded sheet flexures. When

using a single beam element per sheet flexure, the model contains 144 elements and 625 degrees of freedom, increasing to 2640 DOF for the model with 3 elements per sheet flexure. Figure 10 shows the support stiffness in z-direction as a function of the end-effector displacement in z-direction, simulated at 11 steps. It can be seen that a single second-order element per sheet flexure is inadequate. Again, the model with a single third-order element per sheet flexure is very close to the converged solution obtained with multiple second-order elements, showing a factor of 6.32 in computation time reduction relative to the 2-element second-order model with similar accuracy. Also, it is noted that with increasing number of elements per sheet flexure, the computation time quickly escalates. While the present work focuses on algorithmic improvements through more efficient discretization, a significant computation time reduction can be expected with more efficient implementations that leverage the sparsity of the equations and parallel processing on multiple cores.

5 Conclusion

This paper presents a third-order stiffness formulation of an initially-straight geometrically non-linear beam element in the generalized strain beam framework. The new two-node element is based on Timoshenko beam theory with the addition of nonuniform torsion and Wagner effects. The element formulation has been derived by means of the Hellinger–Reissner mixed variational principle and a specific set of interpolation functions. The interpolation of the warping bimoment is based on the differential equation solution with hyperbolic functions. The included third-order effects play a significant role in the description of the in-plane stiffness of wide and thin rectangular beams when deformed out of plane. Numerical simulations of precision mechanism examples that rely on in-plane stiffness show that a single third-order element per sheet flexure can already yield adequate results, which otherwise would have required at least twice as many second-order elements. Hence, the number of degrees of freedom can be reduced, and larger systems can be simulated or optimized. The comparison with two models of 24 and 288 flexible elements demonstrates a reduction in computation time by factors of 3 and 6, respectively.

Appendix A Hyperbolic torsion angle solution

The full expression for angle ϕ_x, as outlined in Sect. 2.2, is given by

$$\begin{aligned}\phi_x = {} & \phi_x^q \frac{\lambda\xi\cosh(\lambda/2) - \sinh(\lambda/2) + \sinh(\lambda/2 - \lambda\xi)}{\lambda\cosh(\lambda/2) - 2\sinh(\lambda/2)} \\ & + LW^p \frac{\operatorname{csch}^2(\lambda/2)}{-4\lambda + 2\lambda^2\coth(\lambda/2)} \times \\ & \qquad \big(\lambda\xi + (\lambda - \lambda\xi)\cosh(\lambda) \\ & \qquad - \lambda\cosh(\lambda - \lambda\xi) - \sinh(\lambda) \\ & \qquad + \sinh(\lambda\xi) + \sinh(\lambda - \lambda\xi)\big) \\ & - LW^q \frac{\operatorname{csch}^2(\lambda/2)}{-4\lambda + 2\lambda^2\coth(\lambda/2)} \times \\ & \qquad \big(\lambda - \lambda\xi + \lambda\xi\cosh(\lambda) \\ & \qquad - \lambda\cosh(\lambda\xi) - \sinh(\lambda) \\ & \qquad + \sinh(\lambda\xi) + \sinh(\lambda - \lambda\xi)\big),\end{aligned} \tag{A1}$$

where $\operatorname{csch}(\xi) = 1/\sinh(\xi)$ denotes the hyperbolic cosecant function, $\coth(\xi) = \cosh(\xi)/\sinh(\xi)$ the hyperbolic cotangent function, and λ the dimensionless parameter $L\sqrt{GJ/(EI_w)}$.

Appendix B Bimoment interpolation

The full expression for the bimoment interpolation, as outlined in Sect. 3.3, is given by

$$\begin{aligned}B = {} & - W^p LGJ \frac{\cosh(\lambda - \lambda\xi)\operatorname{csch}(\lambda)}{\lambda} \\ & + W^q LGJ \frac{\cosh(\lambda\xi)\operatorname{csch}(\lambda)}{\lambda} \\ & + \widetilde{M}_x L \frac{\operatorname{sech}(\lambda/2)\sinh(\lambda/2 - \lambda\xi)}{\lambda} \\ & + \widetilde{M}_y^p L \Big\{ \phi_z^p \left(24 + 6\lambda^2 - 18\lambda^2\xi + 12\lambda^2\xi^2\right) \\ & + \phi_z^q \left(24 + 2\lambda^2 - 12\lambda^2\xi + 12\lambda^2\xi^2\right) \\ & + \left[-6\phi_z^p - 12\phi_z^q\right]\cosh(\lambda\xi)\operatorname{csch}(\lambda)\lambda \\ & + \left[\phi_z^p\left(-18 - \lambda^2\right) - 12\phi_z^q\right] \times \\ & \cosh(\lambda - \lambda\xi)\operatorname{csch}(\lambda)\lambda \Big\} \\ & + \widetilde{M}_y^q L \Big\{ \phi_z^p \left(24 + 2\lambda^2 - 12\lambda^2\xi + 12\lambda^2\xi^2\right) \\ & + \phi_z^q \left(24 - 6\lambda^2\xi + 12\lambda^2\xi^2\right) \\ & + \left[-12\phi_z^p + \phi_z^q(-18 - \lambda^2)\right] \times \cosh(\lambda\xi)\operatorname{csch}(\lambda)\lambda \\ & + \left[-12\phi_z^p - 6\phi_z^q\right] \times \cosh(\lambda - \lambda\xi)\operatorname{csch}(\lambda)\lambda \Big\},\end{aligned} \tag{B2}$$

where $\operatorname{sech}(\xi) = 1/\cosh(\xi)$ denotes the hyperbolic secant function.

Acknowledgements This research was funded by the Innovative Research Incentives Scheme VIDI (Stichting voor de Technische Wetenschappen) (14152 NWO TTW) of the Ministry of Education, Culture and Science of the Netherlands.

References

1. Aarts RGKM, Meijaard JP, Jonker JB (2012) Flexible multibody modelling for exact constraint design of compliant mechanisms. Multibody Sys Dyn 27(1):119–133
2. Alfano G, de Sciarra F (1996) Mixed finite element formulations and related limitation principles: a general treatment. Comput Methods Appl Mech Eng 138(1–4):105–130
3. Alsafadie R, Hjiaj M, Battini JM (2011) Three-dimensional formulation of a mixed corotational thin-walled beam element incorporating shear and warping deformation. Thin-Walled Struct 49(4):523–533
4. Antman SS (1972) The Theory of Rods. Linear Theories of Elasticity and Thermoelasticity. Springer, Berlin Heidelberg, Berlin, pp 641–703
5. Belytschko T, Glaum LW (1979) Applications of higher order corotational stretch theories to nonlinear finite element analysis. Comput Struct 10(1–2):175–182
6. Besseling JF (1964) The complete analogy between the matrix equations and the continuous field equations of structural analysis. International Symposium on Analogue and Digital Techniques Applied to Aeronautics, 223–242
7. Besseling JF (1974) Non-linear analysis of structures by the finite element method as a supplement to a linear analysis. Comput Methods Appl Mech Eng 3(2):173–194
8. Cardona A, Geradin M (1988) A beam finite element non-linear theory with finite rotations. Int J Numer Meth Eng 26(11):2403–2438
9. Cosserat E, Cosserat F (1909) Théorie Des Corps Déformables. Librarie scientifique A, Hermann et fils, Paris
10. Cowper GR (1966) The shear coefficient in Timoshenko's beam theory. J Appl Mech 33(2):335–340
11. Crisfield M (1990) A consistent co-rotational formulation for non-linear, three-dimensional, beam-elements. Comput Methods Appl Mech Eng 81(2):131–150
12. Crisfield M (1991) Non-Linear Finite Element Analysis of Solids and Structures. John Wiley & Sons
13. Cullimore MSG (1949) The shortening effect - A non-linear feature of pure torsion. Engineering Structures, 153–164
14. Eastman FS (1935) Flexure pivots to replace knife edges and ball bearings. In: Engineering Experiment Station Bulletin 86
15. Felippa CA (1989) Parametrized multifield variational principles in elasticity: i mixed functionals. Commun Appl Numer Methods 5(2):79–88
16. Felippa CA (1994) A survey of parametrized variational principles and applications to computational mechanics. Comput Methods Appl Mech Eng 113(1–2):109–139
17. Felippa CA, Haugen B (2005) A unified formulation of small-strain corotational finite elements: i Theory. Computer Methods Appl Mech Eng 194(21–24):2285–2335
18. Ibrahimbegović A (1995) On finite element implementation of geometrically nonlinear Reissner's beam theory: three-dimensional curved beam elements. Comput Methods Appl Mech Eng 122(1–2):11–26
19. Jelenić G, Saje M (1995) A kinematically exact space finite strain beam model — finite element formulation by generalized virtual work principle. Comput Methods Appl Mech Eng 120(1–2):131–161
20. Jones RV (1956) A parallel-spring cross-movement for an optical bench. J Sci Instrum 33(7):279–280
21. Jonker B (1989) A finite element dynamic analysis of spatial mechanisms with flexible links. Comput Methods Appl Mech Eng 76(1):17–40
22. Jonker JB (2021) Three-dimensional beam element for pre- and post-buckling analysis of thin-walled beams in multibody systems. Multibody Sys Dyn 52(1):59–93
23. Jonker JB, Meijaard JP (1990) SPACAR—Computer program for dynamic analysis of flexible spatial mechanisms and manipulators. In Multibody systems handbook, Berlin Heidelberg, pp 123–143
24. Jonker JB, Meijaard JP (2013) A geometrically non-linear formulation of a three-dimensional beam element for solving large deflection multibody system problems. Int J Non-Linear Mech 53:63–74
25. Jonker JB, Aarts RGKM, van Dijk J (2008) A linearized input–output representation of flexible multibody systems for control synthesis. Multibody Sys Dyn 21(2):99–122
26. Li W, Ma H, Gao W (2017) Geometrically exact curved beam element using internal force field defined in deformed configuration. Int J Non-Linear Mech 89:116–126
27. Love AEH (1927) A Treatise on the Mathematical Theory of Elasticity, 4th edn. Cambridge University Press
28. Meier C, Popp A, Wall WA (2019) Geometrically exact finite element formulations for slender beams: Kirchhoff–Love theory versus Simo-Reissner theory. Arch Computa Methods Eng 26(1):163–243
29. Meijaard JP (1996) Validation of flexible beam elements in dynamics programs. Nonlinear Dyn 9(1–2):21–36
30. Meijaard JP (2014) Fluid-conveying flexible pipes modeled by large-deflection finite elements in multibody systems. J Computat Nonlinear Dyn 9(1):011008
31. Meijaard JP (2015) The importance of imperfections in leaf-spring flexures for the support stiffness. Procedia IUTAM 13:82–89
32. Meijaard JP (2018) A method for calculating and continuing static solutions for flexible multibody systems. J Comput Nonlinear Dyn 13(7):071002
33. Meijaard JP (2023) An extended modelling technique with generalized strains for flexible multibody systems. Multibody Sys Dyn 57(2):133–155
34. Nachbagauer K (2014) State of the art of ANCF elements regarding geometric description, interpolation strategies, definition of elastic forces, validation and the locking phenomenon in comparison with proposed beam finite elements. Arch Comput Methods Eng 21(3):293–319
35. Naves M, Aarts RGKM, Brouwer DM (2019) Large stroke high off-axis stiffness three degree of freedom spherical flexure joint. Precis Eng 56:422–431
36. Naves M, Aarts RGKM, Brouwer DM (2019) Maintaining high support stiffness. Mikroniek 59(3):17–21
37. Nijenhuis M, Meijaard JP, Brouwer DM (2020) A spatial closed-form nonlinear stiffness model for sheet flexures based on a

mixed variational principle including third-order effects. Precis Eng 66:429–444
38. Reissner E (1972) On one-dimensional finite-strain beam theory: the plane problem. Zeitschrift für angewandte Mathematik und Physik ZAMP 23(5):795–804
39. Reissner E (1973) On one-dimensional large-displacement finite-strain beam theory. Stud Appl Math 52:87–95
40. Santos HAFA, Pimenta PM, de Almeida JPM (2010) Hybrid and multi-field variational principles for geometrically exact three-dimensional beams. Int J Non-Linear Mech 45(8):809–820
41. Santos HAFA, Pimenta PM, Almeida JPM (2011) A hybrid-mixed finite element formulation for the geometrically exact analysis of three-dimensional framed structures. Comput Mech 48(5):591–613
42. Schulz M, Filippou FC (1998) Generalized warping torsion formulation. J Eng Mech 124(3):339–347
43. Schwab AL (2002) Dynamics of flexible multibody systems. PhD thesis, Delft University of Technology
44. Schwab AL, Meijaard JP (2010) Comparison of three-dimensional flexible beam elements for dynamic analysis: classical finite element formulation and absolute nodal coordinate formulation. J Comput Nonlinear Dyn 5(1):011010
45. Shabana AA, Yakoub RY (2001) Three dimensional absolute nodal coordinate formulation for beam elements: theory. J Mech Des 123(4):606–613
46. Simo J (1985) A finite strain beam formulation. the three-dimensional dynamic problem. part I. Comput Methods Appl Mech Eng 49(1):55–70
47. Simo J, Vu-Quoc L (1986) A three-dimensional finite-strain rod model part II: computational aspects. Computer Method Appl Mech Eng 58(1):79–116
48. Simo JC, Armero F (1992) Geometrically non-linear enhanced strain mixed methods and the method of incompatible modes. Int J Numer Meth Eng 33(7):1413–1449
49. Slocum AH (1992) Precision Machine Design. Prentice Hall, Englewood Cliffs, New Jersey
50. Smith ST (2000) Flexures: Elements of Elastic Mechanisms. CRC Press
51. Tang Y, Tian Q, Hu H (2022) Efficient modeling and order reduction of new 3D beam elements with warping via absolute nodal coordinate formulation. Nonlinear Dyn 109(4):2319–2354
52. Timoshenko S, Gere JM (1961) Theory of Elastic Stability, second, edition. McGraw-Hill, McGraw-Hill
53. Trahair NS (2005) Nonlinear elastic nonuniform torsion. J Struct Eng 131(7):1135–1142
54. Vlasov VZ (1961) Thin-Walled Elastic Beams. Israel Program for Scientific Translations
55. Wang T, Mikkola A, Matikainen MK (2022) An overview of higher-order beam elements based on the absolute nodal coordinate formulation. J Comput Nonlinear Dyn 17(9):091001
56. Washizu K (1982) Variational Methods in Elasticity and Plasticity, third (edn). Pergamon Press
57. Weiss H (2002) Dynamics of geometrically nonlinear rods: II. numerical methods and computational examples. Nonlinear Dyn 30:383–415
58. Yakoub RY, Shabana AA (2001) Three dimensional absolute nodal coordinate formulation for beam elements: implementation and applications. J Mech Des 123(4):614–621